JOURNAL OF PROPULSION AND POWER
Vol. 32, No. 2, March-April 2016

Vortex-Lift Mechanism in Axial Turbomachinery with Periodically Pitched Stators

Lin Du* and Xiaofeng Sun†
Beihang University, 100191 Beijing, People's Republic of China
and
Vigor Yang‡
Georgia Institute of Technology, Atlanta, Georgia 30332

DOI: 10.2514/1.B35859

Conventional aerodynamic theory of lift is based on the Kutta–Joukowski condition, in which the lift and drag coefficients are predicted based on the assumption that flow is attached and steady-state. Recent research on insect flight indicates, however, that the unsteady motion of a wing can generate much higher unsteady aerodynamic force through the flow induced by the shedding vortices. In the present work, therefore, we propose a novel type of stage consisting of rotor and periodically pitched stator to take advantage of unsteady vortex lift. The numerical results suggest that the flowfield around the leading and trailing edges of the blades are substantially modified by the interactions between the rotor and pitching stator. Several transient lift peaks can be generated for each period. If an appropriate pitching phase is chosen for the stator, stage performance can be improved through unsteady lift mechanism effects.

Nomenclature

A	=	pitching amplitude coefficient of stator blade
C_d	=	drag coefficient
C_l	=	lift coefficient
C_p	=	static pressure coefficient
c	=	chord
h	=	enthalpy
F_x, F_y	=	boundary forces
$\boldsymbol{f}$	=	boundary force density
l	=	distance from points O_1/O_2 to leading edge of blades
Ma	=	axial Mach number
O_1, O_2	=	reference points on rotor and stator blades
P_r	=	pitch of rotor
P_s	=	pitch of stator
p^*	=	total pressure
Re	=	Reynolds number
T_{rs}	=	P_r/V
T_{sr}	=	P_s/V
U	=	velocity of incoming flow at inlet
V	=	moving velocity of rotor blade
α_1, α_2, α_3	=	stagger angle
Γ_1	=	circulation around rotor
Γ_2	=	circulation of shedding vortex
δ	=	axial gap
μ	=	dynamic viscosity
ρ	=	density
τ	=	time delay of pitching of stator blade
ϕ	=	U/V, flow coefficient
ψ	=	time-averaged total-to-total pressure rise coefficient
ψ_t	=	unsteady total-to-total pressure rise coefficient

Received 22 April 2015; revision received 17 September 2015; accepted for publication 19 September 2015; published online 16 December 2015.

*Ph.D., Postdoc Research Fellow, School of Jet Propulsion; lindu_buaa@sina.cn.

†Professor, School of Jet Propulsion; sunxf@buaa.edu.cn (Corresponding Author).

‡William R. T. Oakes Professor, School of Aerospace Engineering; victor.yang@aerospace.gatech.edu.

I. Introduction

AIRCRAFT gas-turbine engines require a high thrust-to-weight ratio, which is mainly realized in the compressor by increasing blade loading and lowering the number of rotor/stator stages. The former is determined by the lift coefficient and velocity on the blade. Within the current design system, the only viable means to improve blade loading appears to be increasing the rotor speed because the margin for improving the lift coefficient is limited, according to existing lift theories. Increasing rotor speed, however, results in severe shock/boundary-layer interactions and flow separation on the blade due to the associated high relative Mach number. Under such conditions, the challenge of enhancing stall characteristics and engine efficiency is formidable.

In the present study, a new lift mechanism with a much higher lift coefficient is developed. The work is motivated by the vortex-lift mechanism of insect flight. This is commonly known as the Weis-Fogh mechanism [1,2], which was discovered in the clap-and-fling motion of a small *Encarsia formosa* by Weis-Fogh [1], as shown in Fig. 1. The Weis-Fogh mechanism results in a kind of vortex lift with an unsteady feature and offers remarkably high loading and maneuverability. Both numerical and experimental investigations [3–9] show that, in the context of insect motion, the aerodynamic principle of hovering is distinct from the conventional aerodynamic mechanisms of a wing. Li and Lu [10] investigated the dynamics of a flapping plate using a viscous vortex-ring model. It is found that the force and power of the flapping plate are dominated by the vortical structures near the body. The impulse of each vortical structure is close to the momentum of the plate transferred to the flow for the formation of such vortical structure.

Another kind of interaction is the fore- and hindwing interaction commonly observed in dragonfly flight [11–19]. Sun and Lan [11] investigated the lift mechanism for a hovering dragonfly using a three-dimensional Navier–Stokes solver with an overset grid method. It was found that the interaction between the two wings reduces the vertical forces on the fore- and hindwings. The same effect was also observed by Wang and Sun [12]. Wang and Russell [17] concluded that the aerodynamic power expended is reduced when the two wings move out of phase, and the force is enhanced when the two wings move in phase. Zhang and Lu [18] found that the interaction between the fore- and hindwing effectively enhanced the lift force and reduced the drag force on the wings compared to two independent wings. In dragonfly flight, high lift coefficients (2–6) were observed, which are difficult to explain using a quasi-steady analysis [14–16]. The present work attempts to improve the performance of a turbomachine by implementing unsteady interactions between the rotor and stator in a manner similar to the fore- and hindwing motions in dragonfly flight.

Establishing this type of unsteady lift mechanism in turbomachinery will require fundamental insight into the formation of vortex lift through the relative motion of blades. The objective of the present study, therefore, is to advance rotor–stator performance through the implementation of the vortex-lift mechanism.

Compared to the rich history of investigation of the unsteady vortex lift mechanism for micro air vehicles, very little attention has been paid to its application in turbomachinery. There are significant practical challenges in imitating hovering flight with rotor/stator blades, given the complicated topological structures and flow motions in turbomachinery, but if the unsteady lift mechanism could be implemented to generate high stage loading, more compact turbomachinery could be developed. Tsutahara et al. [20,21] attempted to apply the Weis-Fogh mechanism to ship propulsion. The resulting model ship [20] can move smoothly with a maximum efficiency of about 75%. Furber and Ffowcs Williams [22] reported that the measured properties of an axial pump are improved when the gap between blade rows is reduced, implying that the improvement is caused by the Weis-Fogh mechanism. Their work, however, only considered steady potential flow. Many flow factors were ignored, including the effects of vortices and viscosity, which play important roles in the generation and development of standing vortices. The underlying mechanism still remains a problem of concern, and a workable way to effectively implement the unsteady lift mechanism in turbomachinery would be of great interest.

In a separate work, we have proposed [23] reducing the axial gap between blade rows as a means of enhancing rotor/stator interaction to generate high unsteady lift and improve the stage loading. In the present work, a novel stage consisting of a rotor and a periodically pitched stator is proposed to further enhance rotor/stator interaction. As depicted in Fig. 2, the motion of rotor blades is conventional, but the stator blades are periodically pitched with a small amplitude $\pm\Delta\alpha$ depending on the position of nearby rotor blades. The interaction between the rotor and stator is enhanced by the motion of the periodically pitched stator in the proposed system. The situation is similar to the fore- and hindwing interaction commonly observed in dragonfly flight, in which the wing motion includes flapping and pitching (Fig. 1 in Wang [16]).

Figure 2 shows the position of rotor blades at two instants $t = NT_{rs}$ and $t = NT_{rs} + \Delta t$ ($N = 1, 2, 3\ldots$). T_{rs} denotes the interval for a stator blade passed by different rotor blades, which is P_r/V. Accordingly, T_{sr} is P_s/V. At $t = NT_{rs}$, the trailing edge of the rotor blade is aligned with the leading edge of the stator blade. The stator blade is periodically pitched around its fixed point, and the angular velocity is prescribed by

$$\begin{cases} \Omega = A(1 - \cos 4\pi t') & -1/2 \le t' < 0 \\ \Omega = -A(1 - \cos 4\pi t') & 0 \le t' < 1/2 \end{cases} \tag{1}$$

where the relative time is defined as

$$t' = \Psi\left(\frac{t-\tau}{T_{rs}} + \frac{1}{2}\right) - \frac{1}{2} \tag{2}$$

where the function Ψ indicates that the decimal part of the value is reserved. τ is the time delay of the pitching of the stator blade, which determines the pitching phase and varies in the range $0\sim T_{rs}$. To investigate the influence of pitching phase, the time delay in Eq. (2) is set to be $\tau = kT_{rs}/8$, and the pitching phase varies in the range $k = 0, 1, \ldots 7$. A is the pitching amplitude coefficient. For $A = 0.25$, Fig. 3 shows the relative time t', Ω, and $\Delta\alpha$ in two periods for $\tau = 0.00$ and $\tau = 0.25T_{rs}$, respectively. The generation and development of vortices around the rotor blade are modulated by the pitching phase and amplitude. The pitching phase determines the relative motion between the rotor and pitching stator. This is the crucial parameter in the present system, similar to the phase between the fore- and the hindwing in dragonfly flight [13,16,17]. The net effect of varying the pitching phase can be either positive or negative. The vortex interaction intensity depends on the pitching amplitude.

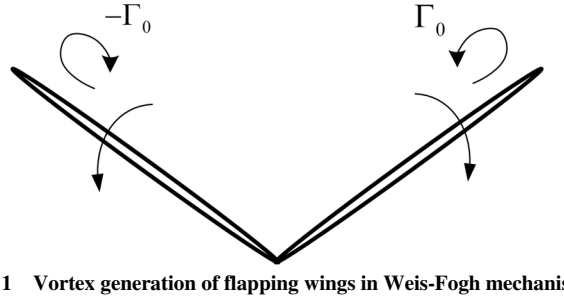

Fig. 1 Vortex generation of flapping wings in Weis-Fogh mechanism.

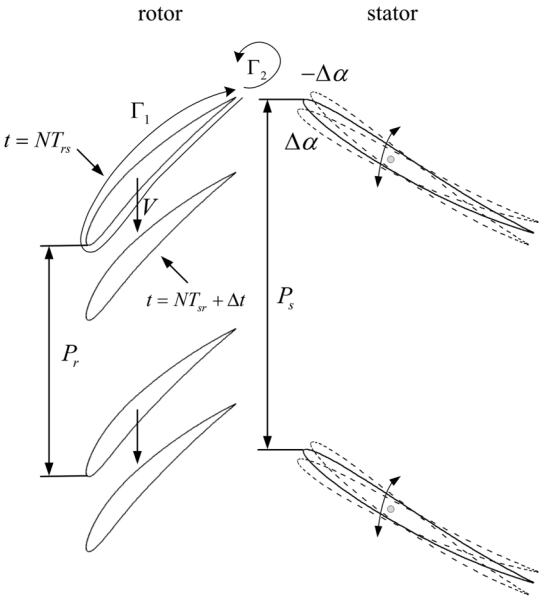

Fig. 2 Schematic diagram of an axial turbomachinery stage consisting of a rotor and a periodically pitched stator.

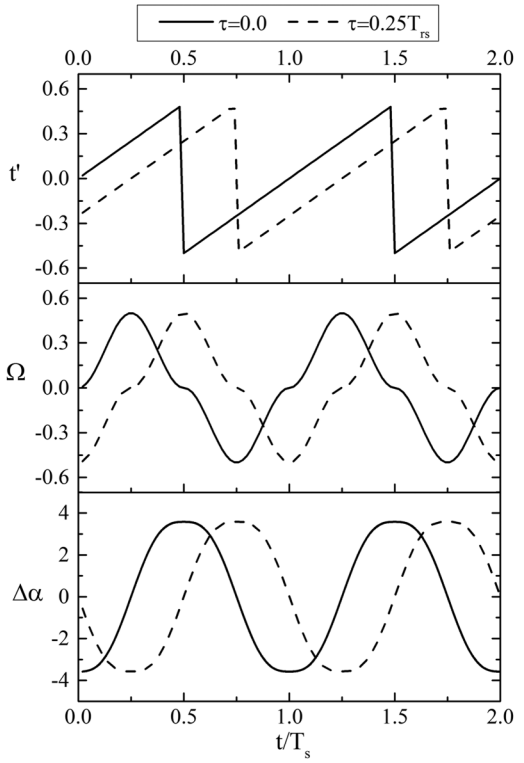

Fig. 3 t', Ω, and $\Delta\alpha$ in two periods for $\tau = 0.00$ and $\tau = 0.25T_{rs}$. Pitching amplitude coefficient $A = 0.25$.

The loading of a rotor blade depends on the circulation around the rotor blade and on the inflow velocity.

In the earlier studies on the Weis-Fogh mechanism [2,5,22], the high unsteady lift generated on the wing/blade was thought to be related to the circulation around the wing and blade surfaces. Maxworthy [3], however, indicated that the circulation around a wing surface alone is actually of opposite sign to that of the shedding vortex. On the basis of Kelvin's theorem, the circulation Γ_1 is influenced by the intensity of the shedding vortex Γ_2. Kelvin's circulation theorem has long been employed to provide qualitative understanding of this phenomenon. At a given instant, if the intensity of the shedding vortex is enhanced by the interaction between rotor and pitching stator, a enhancement of circulation may occur on the rotor blade. The stage loading then increases under the same inflow conditions. Recent work [24–26] on wake/blade row interaction has studied the effect of wake decay and generation of entropy on stage efficiency. The variation of efficiency is thought to be related to the wake recovery theory proposed by Smith [27]. Zheng et al. [28] proposed that the aerodynamic performance of a compressor can be enhanced by the transition of an unsteady vortical flow over the blade row from a chaotic to an orderly state. In their study, the upstream wake from a stator blade row was represented by the total pressure fluctuation. The loss coefficient can be effectively reduced if the excitation frequency is optimized and the excitation amplitude is large enough. The study conducted by Li and Lu [10] showed that the force and power generated by a flapping wing are closely linked to the local vortical structures. To offer a quantitative analysis of the whole configuration, the present numerical work deals with the evolution of distributions of pressure, velocity, and vorticity during the rotor/pitching-stator interaction. The relationships among unsteady vortices, rotor lift coefficient, and stage pressure rise are examined by means of comprehensive numerical simulations.

The mathematical treatment of the interaction between a rotor and a periodically pitched stator involves moving boundaries. Conventional numerical schemes [29–33], using either structured or unstructured grids, can be used to discretize the governing equations on a curvilinear grid system that conforms to the boundaries. One persistent obstacle in the research on the rotor/stator interaction, however, lies in the application of two different coordinate systems (a relative coordinate system for the rotor and a fixed coordinate system for the stator), which inevitably results in a data exchange between the two coordinate systems by mixing or interpolation. Approaches to this problem are described in [29–33].

These challenges become even more daunting in the present study of interaction involving a rotor and a periodically pitched stator. The numerical grids associated with the pitching stator must be generated dynamically, thereby substantially increasing the computational burden. To resolve these problems, a new computational strategy will be required.

Several computational methods are available to simulate flow problems with moving boundaries. In recent decades, the volume-of-fluid [34], level-set [35], vortex [36–38], and immersed-boundary (IB) methods [39–41] have been developed and applied. One characteristic of these methods is that grid regeneration is avoided even when boundaries move arbitrarily, and so the computational cost is reduced. The IB method is selected in the present work because of its easy integration into the scheme developed by Jorgenson and Chima [31] and Chima [32], in which the circumferential flow can be directly included in a cylindrical coordinate system. The overall approach allows for simulations of flow with complex topologies and moving boundaries on simple orthogonal meshes. Only a single zone is needed, and the difficulties of generating multiple grids and treating interfacial boundaries are eliminated. The present method has been used in previous work by Zhong and Sun [42] and by Du et al. [43,44] to study fluid–structure interactions, capturing complicated nonlinear coupling and flow transition phenomena. The same authors have used this method to simulate the unsteady flow of a modulation fan with pitching blades [45], which can generate low-frequency sound at high sound pressure levels. The numerical results agreed very well with the measurements reported by Park and Garcés [46]. Finally, the present method has also been used to investigate the effect of shedding vortices in the process of rotor/stator interaction in turbine engines when the axial gap between blade rows is reduced [23].

The aerodynamic structures and flow characteristics of a stage consisting of a rotor and a periodically pitched stator are considered in this paper. Both incompressible laminar and compressible turbulent flows are considered. Both periodically pitched stator blades after rotor blades and inlet guide vanes (IGVs) are examined. The numerical results suggest that, if appropriate pitching phase is chosen, repeated lift peaks will appear on the rotor blades due to the optimal interaction between the rotor and pitching stator blades, and the average stage loading can thus be enhanced. In the authors' opinion, development of such a rotor/pitching-stator configuration offers the potential for the application of unsteady vortex lift in turbomachinery. The flow physics and mechanical structures associated with rotors and periodically pitched stators in a compressor is much more complex than those with the fore- and hindwings of a dragonfly. The rotary subwoofer with periodically pitched rotor blades designed by Park and Garcés [46], nonetheless, showed the technological feasibility of such a rotor/pitched-stator structure.

II. Governing Equations

The immersed-boundary (IB) method is applied to solve Chima's quasi-three-dimensional model [31,32] for treating the unsteady flowfield associated with the rotor/stator interaction, as shown schematically in Fig. 4. The geometry of concern is depicted in Fig. 5, where m and θ are coordinates of the stream surface. The radius and thickness of the stream surface are denoted by $r(m)$ and $h(m)$, respectively, and can be considered as known functions of m. In the present study, $r(m)$ and $h(m)$ are assumed to be constants to facilitate theoretical insight without increasing geometric complexity. The conservation equations of mass and momentum for incompressible flows can be written as

$$\left(\frac{\partial u_m r}{\partial m} + \frac{\partial u_\theta}{\partial \theta}\right) = 0 \tag{3a}$$

$$\rho\frac{\partial u_m r}{\partial t} + \rho\frac{\partial u_m^2 r}{\partial m} + \rho\frac{\partial u_\theta u_m}{\partial \theta} = -\frac{\partial pr}{\partial m} + F_m r + \left(\frac{\partial r\sigma_{11}}{\partial m} + \frac{\partial \sigma_{12}}{\partial \theta}\right) + \sum_{l=1}^{M} F_{x,l} \tag{3b}$$

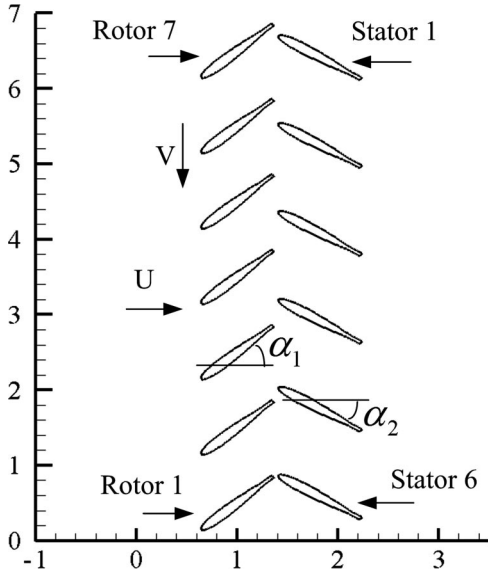

Fig. 4 Schematic diagram of rotor and periodically pitched stator. NACA 0012 blade. α1= 45 deg, α2 = -35 deg, $d = 0.82$, $\delta = 0.05c$.

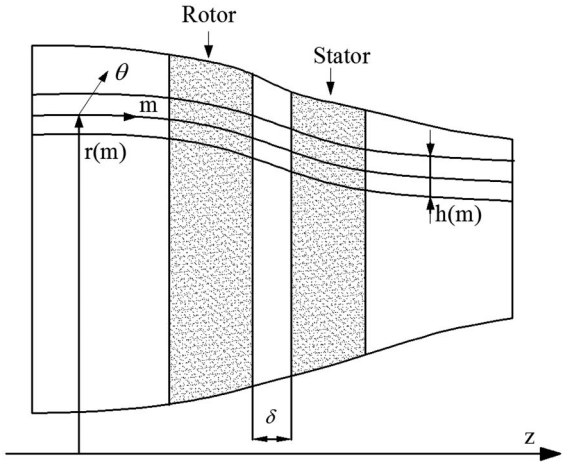

Fig. 5 Quasi-three-dimensional stream surface for a compressor rotor/stator stage.

$$\rho\frac{\partial u_\theta r}{\partial t}+\rho\frac{\partial u_\theta u_m r}{\partial m}+\rho\frac{\partial u_\theta^2}{\partial\theta} = -\frac{\partial p}{\partial\theta}+F_\theta r+\left(\frac{\partial r\sigma_{12}}{\partial m}+\frac{\partial\sigma_{22}}{\partial\theta}\right)+\sum_{l=1}^{M}F_{y,l} \quad (3c)$$

where

$$\sigma_{11}=\frac{2\mu\partial u_m}{\partial m},\qquad \sigma_{12}=\mu\left(\frac{\partial u_m}{r\partial\theta}+\frac{\partial u_\theta}{\partial m}\right),\qquad \sigma_{22}=\frac{\partial 2\mu u_\theta}{r\partial\theta} \quad (4)$$

To solve the governing Eq. (3), the immersed-boundary method is implemented to satisfy the no-slip boundary condition on blades. The details of the numerical scheme and many aspects of the present method can be found in the work of Du et al. [23].

III. Incompressible and Laminar Flow

Most of the existing research on vortex lift mechanisms has focused on the hovering motion of a wing in the low-Reynolds-number regime. We begin our study, therefore, with a consideration of the unsteady lift mechanism in incompressible and laminar flows in the low-Reynolds-number regime. The NACA 0012 airfoil is studied; the ratio between the rotor and stator blades is 7:6, as shown in Fig. 4.

A. Stage with Stationary Stator Blades

Stage characteristics are first investigated for stationary stator blades. The dimensionless time-averaged total-to-total pressure rise coefficient is used to characterize the performance of the rotor/stator stage, defined as

$$\psi(\phi)=\frac{\Delta p^*}{\rho V^2/2}=\frac{p^*_{\text{outlet}}-p^*_{\text{inlet}}}{\rho V^2/2} \quad (5)$$

where p^*_{inlet} and p^*_{outlet} are time-averaged total pressure at the inlet and outlet of the stage, respectively. $\phi=\text{U}/V$ is the flow coefficient. ψ_t denotes the unsteady total-to-total pressure rise coefficient. A grid-independence and temporal-convergence study was performed, and the results suggest that spatial resolution $N_x\times N_y=832\times 512$ and time step $\Delta t=4\times 10^{-4}$ offer both computational accuracy and efficiency. Several parameters are defined: c is the chord of the airfoil; x_{O_1},x_{O_2} are the axial coordinates of points O_1 and O_2; $d=x_{O_2}-x_{O_1}$; α_1, α_2 are the initial stagger angles of the rotor and stator; U is the velocity of the inflow; V is the rotor moving velocity; δ is the axial gap for the initial stagger angle. Points O_1 and O_2 are the reference points on the rotor and stator blades, and l_1/l_2 are the distances from points O_1/O_2 to the leading edge of the blades, as shown in Fig. 6. The Reynolds number is defined by $Re=\rho|V|c/\mu$. Each stator blade is periodically pitched around its fixed point O_2.

The axial gap for the initial stagger angle is 5% of the chord. Figure 7 shows the characteristic curve of the stage. The stage performance varies with the flow coefficient and reaches a peak value at $U/V=0.35$. We then ask whether such a rotor/stator system can achieve a higher rise of stage total pressure by means of stator movement.

B. Stage with Periodically Pitched Stator Blades

A periodically pitched stator placed after the rotor is examined. The rotor blades translate at fixed velocity V. It is easy to calculate that $T_{rs}=1.0$ and $T_{sr}=7/6$ in this example. The stator blades, as discussed in Sec. I, periodically pitch around a fixed point O_2, and the angular velocity is prescribed by Eq. (1). To investigate the influence of pitching phase, the time delay in Eq. (2) is set to be $\tau=kT_{rs}/8$, and the pitching phase varies with $k=0,1,\ldots 7$. For $A=0.25$, the pitch range is -28 to -35 deg. Figure 8 shows the variation of ψ versus pitching phase with $U/V=0.35$. Compared to the situation with a stationary stator ($\psi=0.337$), the pressure rise increases when

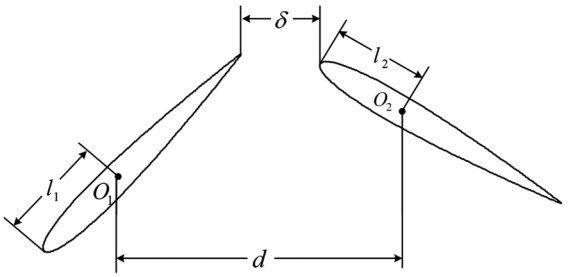

Fig. 6 Reference points O_1, O_2 on blades, $d=x_{O_2}-x_{O_1}$.

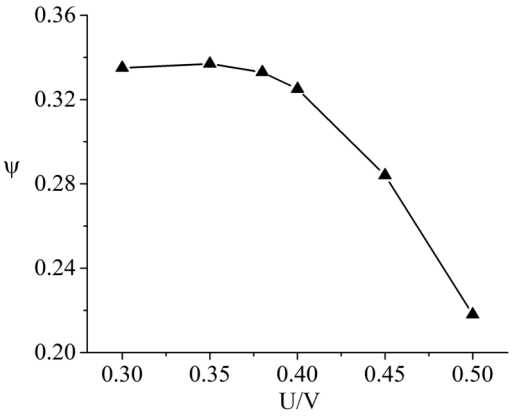

Fig. 7 Characteristic curve of stage (stationary stator, $Re=500$).

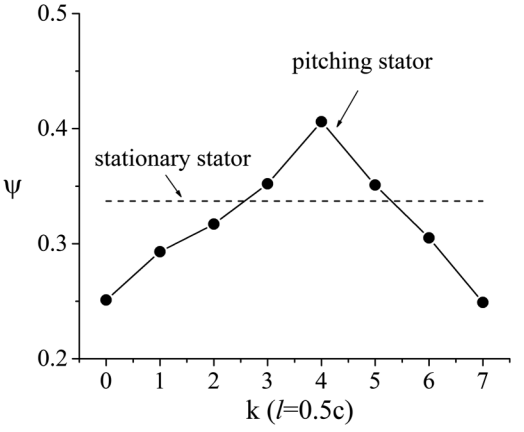

Fig. 8 Average total pressure rise versus pitching phase of periodically pitched stator ($U/V=0.35$, $l=0.5c$).

the pitching phase is $k = 3, 4, 5$. The motion of the pitching stator, however, has a negative effect for the other pitching phases because the stage pressure rise decreases. For $k = 4$, the value increases by about 20.4%. The stage loading is mainly determined by the rotor because the energy used to drive the pitch motion of the stator blade is very low (less than 1% of that of the rotor blade in this example). The increase in the stage total pressure rise is mainly attributed to the fact that the average loading on rotor blades is enhanced.

Three cases ($k = 4$, stationary stator, and $k = 0$) are investigated to determine the influence of the stator motion on the stage loading, especially with regard to the lift coefficients on the rotor blade. Figure 9 shows that the forces on the rotor blades are sensitive to the pitching phase of the stator blades. Clear differences exist among the three cases, even though the essential trends remain the same. Compared to the stationary stator, the lift coefficient has three distinct peaks in every period T_{sr} for pitching phase $k = 4$, at times $t = 0.40$, 0.80, and $0.95T_{sr}$ (NT_{sr} is omitted). Although each peak is short, the rotor blades interact with the stator blades, and lift peaks are generated continuously (enhancing average stage loading). The maximum lift coefficient is 0.89 for $k = 4$, as compared to 0.62 for the case with stationary stators. Compared with the results of stationary stators, the case with $k = 4$ leads to increases of about 20% in both the average stage pressure rise and lift coefficients, suggesting a positive correlation between the stage loading and total pressure rise.

Deep troughs in the lift coefficient are observed for pitching phase $k = 0$. The net effect of the stator movement is negative with this pitching phase. The average lift coefficients are 0.41, 0.26, and 0.34 for $k = 4$, $k = 0$, and the stationary stator, respectively. The pitching phase, namely the time delay, must be optimized to obtain a positive net effect from the interaction between the rotor and periodically pitched stator.

Figure 10 shows the distribution of the static pressure coefficient along the surface of the rotor blade at $t = 0.4T_{sr}$, defined as

$$C_p = \frac{p_{\text{static}} - p_{\text{staticinlet}}}{\rho V^2/2} \tag{6}$$

The distribution of static pressure on the rotor surface is greatly influenced by the motion of the stator blade. The trailing edge of blade is described by two close points with same relative coordinate at $x/c = 1$. A sudden drop of the pressure between the two points at the trailing edge is observed for $k = 0$ because of the occurrence of flow separation. The pressure difference between the pressure and suction surfaces increases along the entire blade, rather than only around the trailing edge. This leads to the enhancement of stage loading and suggests that the effect of the periodically pitched stator blades is not confined to the blade edges but is distributed throughout the whole domain.

Figure 11 shows the vorticity fields for pitching phase $k = 4$ and stationary stator $\alpha^2 = -35$ deg at times $t = 0.40$, 0.80, and $0.95T_{sr}$, respectively. The shedding vortices around the trailing edge of rotor are strengthened by the motion of the pitching stator at these instants. It is noted that the vorticity is nonzero on the blades in Fig. 11. For the rotating rigid body, the whole solid domain will be filled with spatially constant vorticity $2\Omega(t)$, where $\Omega(t)$ is the angular velocity. As described with reference to Fig. 2 and discussed in Sec. I, because of the continuous interaction between rotor and pitching stator, the stage loading increases with the enhancement of shedding vortices. As reported by Li and Lu [10], the force generated on the blade is primarily determined by the vortical structure near the body. In the present study, the shedding vortical structures are enhanced by the rotor/pitching-stator interaction. The relation between unsteady vortex shedding and lift coefficients on the rotor blade is confirmed by the results shown in Figs. 9 and 11. The lift peaks in Fig. 9 are accompanied by stronger shedding vortices from the rotor-blade trailing edge as shown in Fig. 11, which suggests that a higher circulation is generated around the blade. The enhancement of the stage pressure rise the rotor/pitching-stator interaction is thus corroborated. Figure 12 shows the unsteady stage total-to-total pressure rise coefficient for three different pitching phases, $k = 0$, 4, and 5. The pressure rise is highest for $k = 4$. Fluctuation also increases, which is not beneficial. $k = 0$ shows low total pressure and high unsteadiness. $k = 5$ offers only slightly better results than the stationary stator. It is found that the relative pitching phase is the crucial parameter in such a rotor/pitching-stator stage. The pitching phase determines whether the net effect of enhanced interaction is positive or negative.

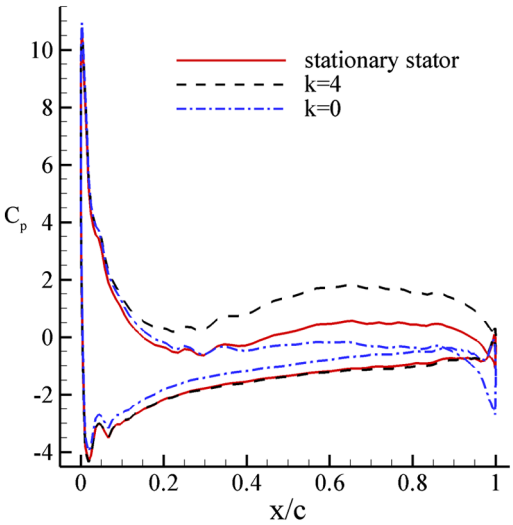

Fig. 10 Pressure coefficients over rotor blade 1 at $t = 0.4T_{sr}$ ($U/V = 0.35, l = 0.5c$).

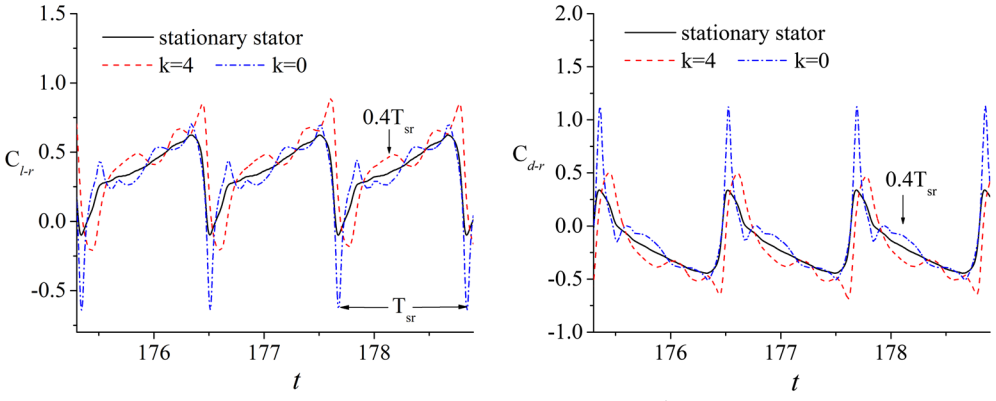

Fig. 9 Comparison of rotor lift and drag coefficients ($U/V = 0.35, l = 0.5c$).

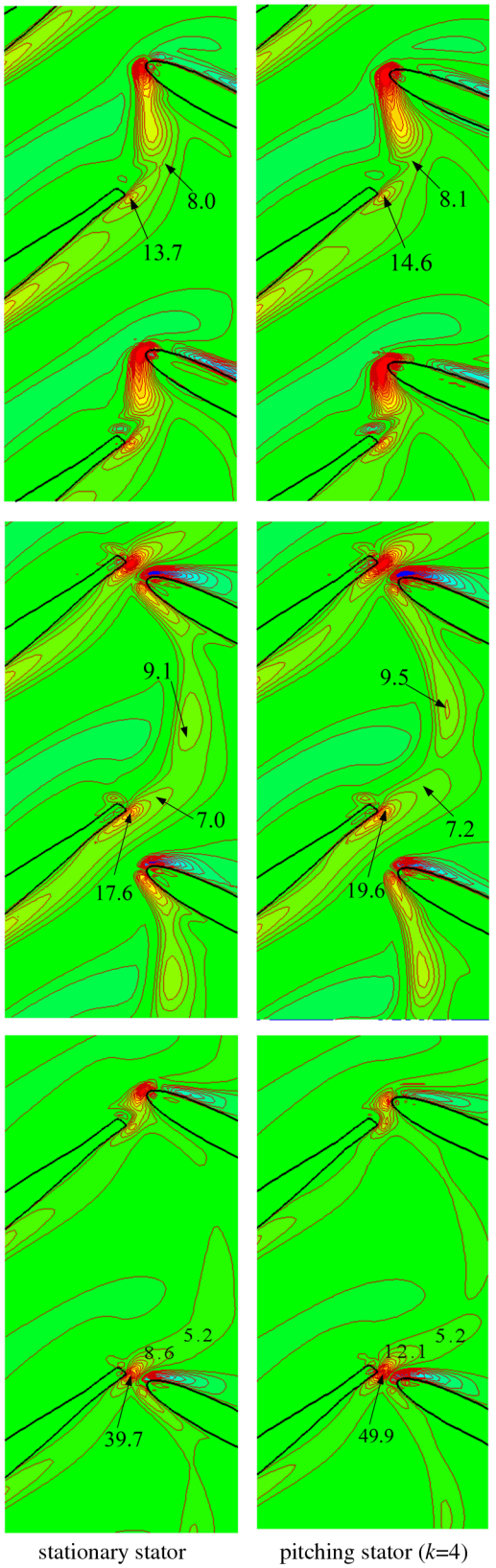

Fig. 11 Comparison of vorticity field around rotor/pitching stator at $t = 0.40$, 0.80, and $0.95T_{sr}$, respectively ($U/V = 0.35$, $l = 0.5c$, $d = 0.82$).

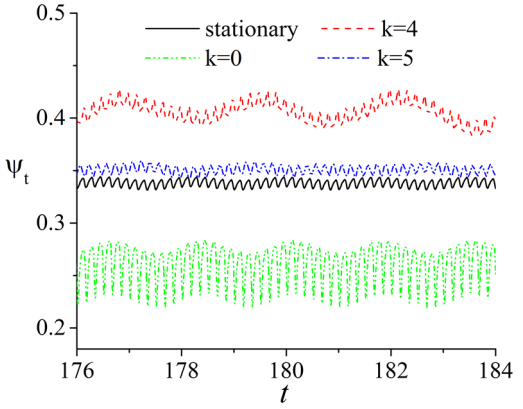

Fig. 12 Unsteady stage total pressure rise for different phases ($U/V = 0.35$, $l = 0.5c$).

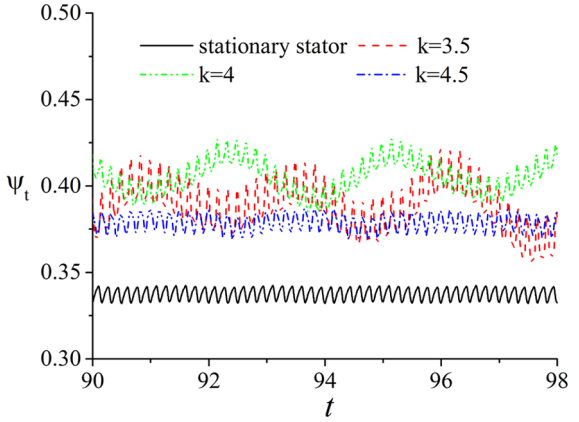

Fig. 13 Optimization of pitching phase ($U/V = 0.35$, $l = 0.5c$).

Given the promising results for $k = 4$, in an effort to optimize pitching phase, further calculations were carried out for $k = 3.5$ and 4.5. Figure 13 shows that the stage pressure rise increases, and the fluctuation is suppressed for $k = 4.5$, as compared to $k = 3.5$ and 4.

For $k = 4.5$, the amplitude of fluctuation is close to the value for the stationary stator. At the same time, the average pressure rise is 0.381, which is 13.1% higher than for the stationary stator. Based on the previous numerical analysis, and taking into account stage loading and fluctuation, $k = 4.5$ may be the best choice for the pitching phase in this example.

The position of the fixed point O_2 was also considered. The parameters from Table 1 were used, but the distance from the blade leading edge was changed to $l = 0.4c$. Figure 14 shows the effect of pitching phase on average total pressure rise for $l = 0.4c$ and $U/V = 0.35$. The variation of ψ with k is sinusoidal. Stage pressure rise increases when $k = 4$, 5, and 6, and the maximum occurs for $k = 5$, which is about 12.5% above the value for the stationary stator. Figure 15 shows a comparison of rotor lift coefficients. The trend is similar to the results of $l = 0.5c$. Three lift peaks are generated in each period due to the rotor/stator interaction. Figure 16 shows ψ_t for different phases. As in the previous examples, the fluctuation amplitude is close to the results for the stationary stator when $k = 5$.

It has been shown clearly that the stage performance is considerably improved by the interaction between the rotor and the pitching stator in these examples. The motion of a periodically pitched stator at an optimal pitching phase enhances the shedding vortex around the rotor blade. As a consequence, several lift peaks are

Table 1 Blade, flow, and geometric parameters in Fig. 4

α_1	α_2	Re	L	V	U	X_{O1}	X_{O2}	d	δ
45 deg	−35 deg	500	$0.5c$	−1	0.3–0.5	1	1.82	0.82	$0.05c$

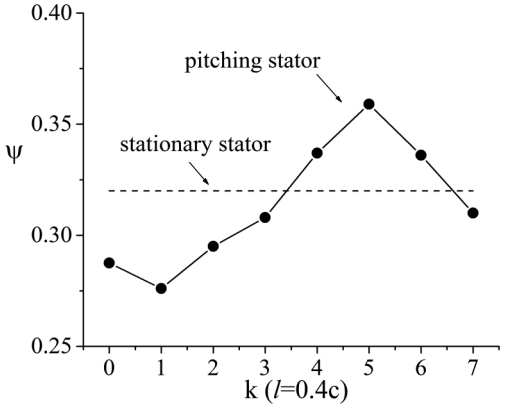

Fig. 14 Average total pressure rise versus k ($U/V = 0.35$, $l = 0.4c$).

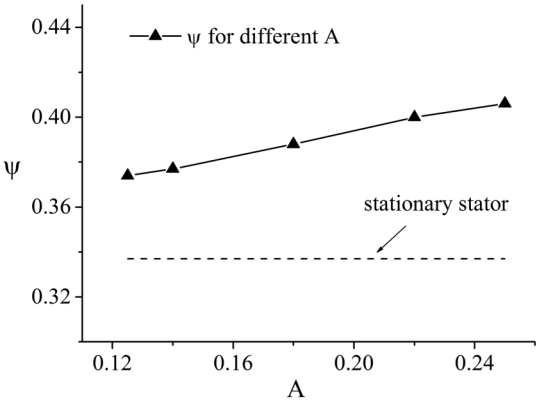

Fig. 17 Effects of pitching amplitude coefficient A of periodically pitched stator ($U/V = 0.35$, $l = 0.5c$, $Re = 500$).

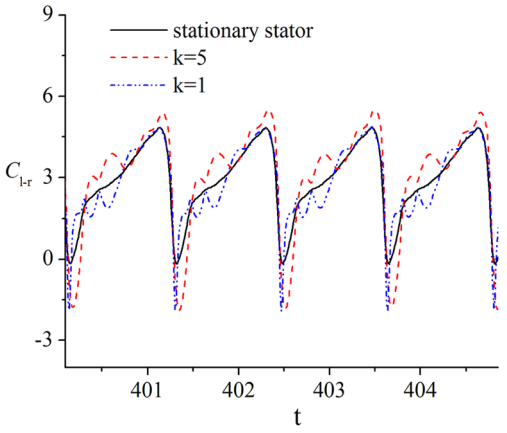

Fig. 15 Comparison of rotor lift coefficients ($U/V = 0.35$, $l = 0.4c$).

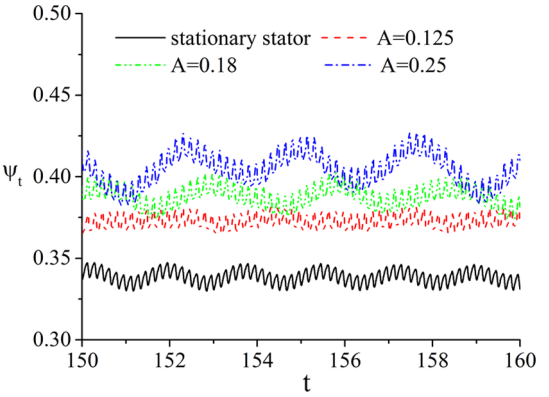

Fig. 18 Unsteady stage pressure rise for different pitching amplitude coefficient A of periodically pitched stator ($U/V = 0.35$, $l = 0.5c$, $Re = 500$).

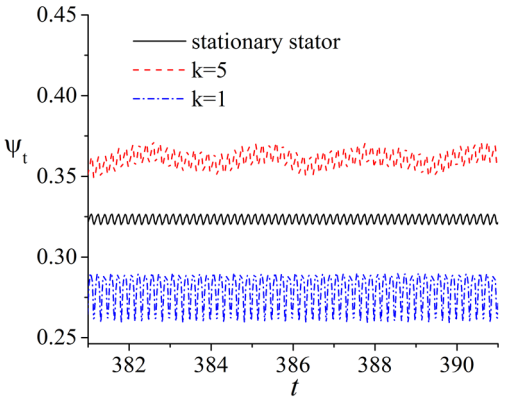

Fig. 16 Unsteady stage total pressure rise for different phases ($U/V = 0.35$, $l = 0.4c$).

obtained in each period. As in the Weis-Fogh mechanism, the unsteady vortex plays an important role in the generation of unsteady lift.

Table 2 Stage total pressure rise for different stagger angles of stator blades

Parameter	Values			
α_2, deg	−28	−31	−35	−28 to −35 ($k = 4.5$)
ψ	0.314	0.323	0.337	0.381
Amplitude of ψ_t	0.031	0.021	0.004	0.006

The pitching range in previous examples is −28 to −35 deg. To confirm the effect of the pitching stator, the stage performance is calculated for the stationary stator with stagger angle −28, −31, and −35 deg. All the other parameters remain identical to those in Table 1. The results are compared with the pitching stator in Table 2. The pitching range is −28 to −35 deg and pitching phase $k = 4.5$. For stationary blades, the stagger angle of $\alpha_2 = -35$ deg produces the best results. This indicates that enhancement of stage performance is not due to optimization of the stagger angle of the stator blades but to the interaction between rotor and pitching stator. Considering the results shown in Table 2, for $k = 4.5$, the pitching stator blades undoubtedly improve the stage performance. The stage pressure rise increases, and the fluctuation is not enhanced.

The previous examples have demonstrated that the stage loading coefficient is enhanced by the periodic motion of the stator if an appropriate pitching phase is imposed. To further investigate the underlying mechanisms, the effects of the pitch amplitude, axial gap, and flow coefficient are examined.

If the pitching amplitude decreases, the process will approach the conditions with a stationary stator. Figure 17 shows the variation of ψ with the pitching amplitude coefficient for $k = 4$. All the other flow and geometric parameters are given in Table 1. The average pressure rise decreases, which is not unexpected, but the effect of the pitching stator is still visible. For $A = 0.125$, the average pressure rise is enhanced by about 11.0%. Figure 18 shows that the fluctuation amplitude of ψ_t is approximately that of the stationary stator. Compared to the vorticity field at the three instants of lift peaks shown in Fig. 11, the value of vortices with $A = 0.125$ is between those of

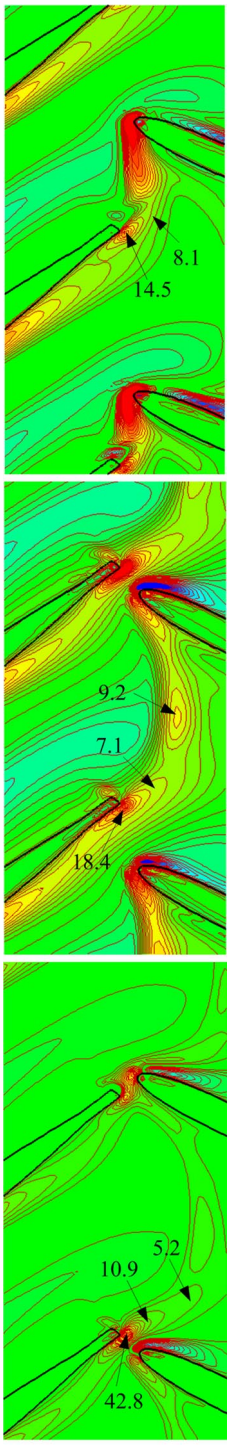

Fig. 19 Vortices field at lift peaks at $t = 0.40$, 0.80l, and $0.95T_{sr}$. Pitching amplitude coefficient $A = 0.125$ and $k = 4$.

the stationary stator and the pitching stator with $A = 0.25$, as shown in Fig. 19.

The effect of the pitching stator is also related to the axial gap between the rotor and stator. The axial gap varies with the value of d, as shown in Fig. 6. The interaction is enhanced when the blade rows are brought closer. Figure 20 shows a comparison of stage pressure rise between stationary stator and pitching stator with different axial gaps. The parameters for the pitching stator are $l = 0.5c$,$A = 0.25$, and $k = 4$. The $\Delta\psi$ between the two characteristic curves decreases if the axial gap increases. Figure 21 compares rotor lift coefficients between stationary and pitching stators with different axial gaps. The increments of average lift coefficient on the rotor blade caused by the motion of the stator are 0.054 and 0.025 for $d = 0.84$ and 0.90, respectively. Figure 22 shows the development of unsteady vortices around the rotor trailing edge for $d = 0.90$. The difference between stationary and pitching stators is lower than those shown in Fig. 11 ($d = 0.82$). This means that the influence of a periodically pitched stator on the rotor blades is weakened if the axial gap increases.

Recall that Fig. 7 shows the characteristic curve for the stationary stator with the parameters in Table 1. It must be asked, then, whether the pitching stator can improve the stage performance for different flow coefficients. Letting $l = 0.5c$, $A = 0.25$, and $k = 4$, the effects of the pitching stator are investigated for several flow coefficients. A comparison of ψ is shown in Fig. 23. It can be seen that the effect of the pitching stator is more marked if the flow coefficient is reduced. The influence of the pitching stator is more evident when the flow condition approaches the off-design point.

The numerical analysis presented here indicates that the rotor/pitching-stator system can significantly enhance stage loading, although the relative phase must be optimized. The use of pitching stator blades changes the vortex distribution around the rotor blades. The lift and drag coefficients on the rotor blades are influenced by unsteady interaction, and the stage loading increases with the enhancement of the shedding vortices. The stage performance is also determined, however, by pitch amplitude, axial gap, and flow coefficient. The flow associated with the rotor/pitching-stator configuration is so complex, however, that it must be considered as a whole system.

C. One-and-a-Half Stage with Periodically Pitched Inlet Guide Vane

In this section, flow passing through 1.5 stages with a periodically pitched IGV and conventional fixed stator is studied. A sketch of the 1.5 stages is shown in Fig. 24. The blades of the first row (pitching IGV) are NACA 0012, and the two aft rows are composed of NACA 4412. The blade ratio is 6:7:5. The parameters for this example are given in Table 3.

First, unsteady flow is investigated with flow coefficient $U/V = 0.45$. The motion of the IGV is given as Eqs. (1) and (2), and the pitching amplitude coefficient is $A = 0.25$. As mentioned previously, the relative phase is very important to stage performance and determines whether the effect of the pitching motion will be positive or negative. The average total pressure rise ψ is plotted in Fig. 25 as a function of pitch phase of the IGV. It can be seen that maximum ψ occurs when $k = 3$, and the stage pressure rise increases

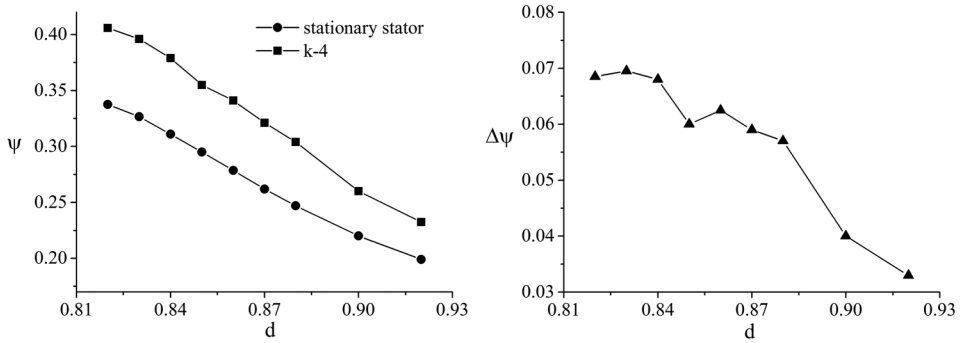

Fig. 20 Comparison of ψ and $\Delta\psi$ versus axial gap for stationary and pitching stator ($l = 0.5c$, $k = 4$).

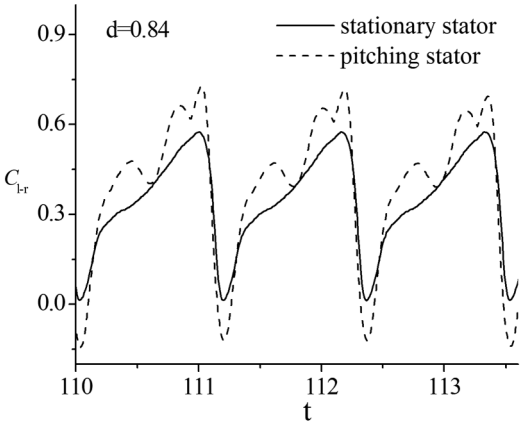

a) d=0.84

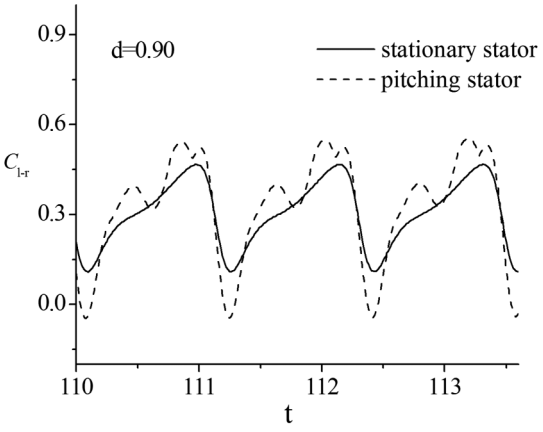

b) d=0.90

Fig. 21 Comparison of rotor lift coefficients for stationary and pitching stator for axial gaps $d = 0.84$ and $d = 0.90$.

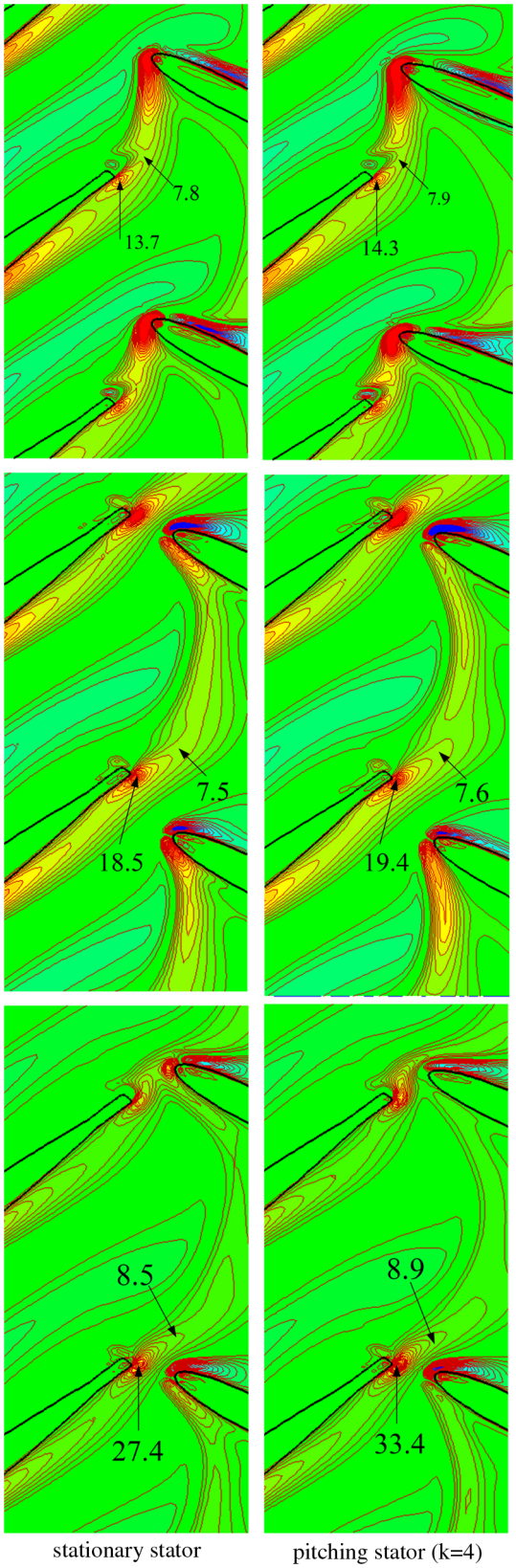

Fig. 22 Comparison of vorticity field around rotor/pitching stator at $t = 0.40$, 0.80, and $0.95T_{sr}$ ($U/V = 0.35$, $l = 0.5c$, $d = 0.90$).

for $k = 2$, 3, 4, and 5. In other words, the pitching IGV can also improve the stage performance, if proper pitching phase is chosen. The effect of the pitching IGV is then investigated for different flow coefficients, with the pitching phase fixed at $k = 3$. Figure 26 shows a comparison of stage pressure rise for stationary IGV and pitching IGV. The stage loading is enhanced even if the flow coefficient is changed, and the pitching IGV is more effective when the flow coefficient increases. This is opposite the trend shown in Fig. 23 for the pitching stator.

Because maximum ψ occurs at about $U/V = 0.3$, this case is investigated in more detail. Figure 26 shows that the average total pressure rise at $U/V = 0.3$ is enhanced by 19.7% by the pitching IGV. Figure 27 plots a comparison of the unsteady stage total pressure rise for the periodically pitched and stationary IGV. The fluctuation amplitude increases from 0.017 to 0.020, due to the motion of the IGV, but the increase is acceptable. Figure 28 shows a comparison of lift and drag coefficients on rotor blades in a given period ($T = 7$). It can be seen that the rotor lift coefficient is enhanced by the pitching IGV. During most of each period, the lift coefficient is enhanced. The average lift coefficients of the rotor blade are 0.295 and 0.258 for the pitching and stationary IGV in a period.

Because the IGV pitching covers a range of -8 to -15 deg, the cases of $\alpha_1 = -8$ deg (smallest axial gap) and $\alpha_1 = -12$ deg are calculated to confirm the positive effect of a pitching IGV. As shown in Table 4, a pitching IGV ($k = 3$) outperforms its stationary counterpart with a stagger angle in the range of -8 to -15 deg. This result proves that the improvement of the stage performance is mainly caused by the optimized pitching IGV rather than by gap reduction.

The flow passing through 1.5 stages is more complex than that in a single stage, and the variation of aerodynamic forces is changed by the interaction between pitching IGV and rotor blades. Based on the average lift coefficient of a rotor blade in a period, the periodically pitched IGV before the rotor can increase the stage loading if the proper pitching phase is chosen. The pitching IGV changes the inflow conditions for the rotor blades, and the aerodynamic

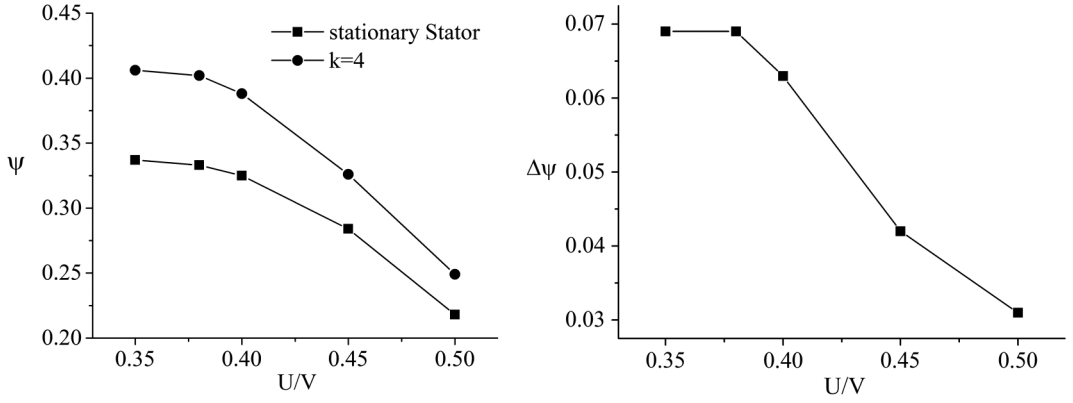

Fig. 23 Comparison of ψ and $\Delta\psi$ with different flow coefficients for stationary and pitching stator ($l = 0.5c$, $k = 4$).

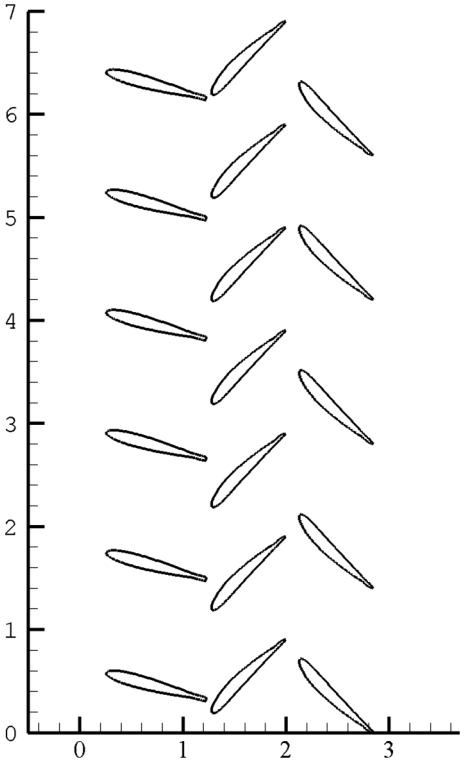

Fig. 24 Sketch of initial relative position of blade rows for 1.5 stages. First row: NACA 0012, two aft rows: NACA 4412. $\alpha_1 = -15$ deg, $\alpha_2 = 45$ deg, $\alpha_3 = -45$ deg, $d_1 = 0.95$, $d_2 = 0.85$, $\delta_1 = 0.05c$, $\delta_2 = 0.13c$.

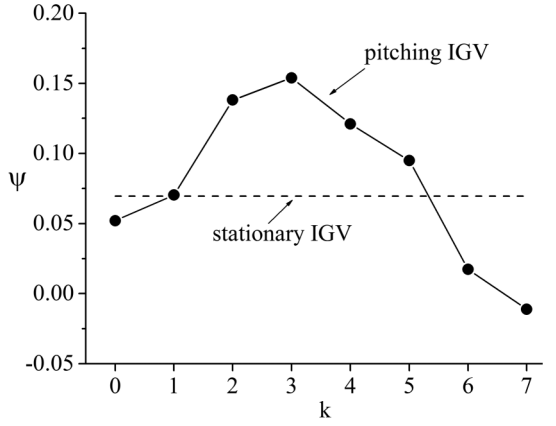

Fig. 25 Average total pressure rise varies with k (pitching IGV).

performance of the stage is improved. For $U/V = 0.3$, the average lift coefficient of a rotor blade is increased by 14.3%, which leads to a 19.7% increase in average stage total pressure rise. It is thought that both the pitching stator after rotor and pitching IGV could be implemented to enhance stage loading if appropriate pitching phase is selected.

IV. Compressible and Turbulent Flow

As mentioned previously, most of the previous research on unsteady lift mechanisms has focused on low-Reynolds-number flows. Turbomachinery, however, usually works with compressible and turbulent flow. To test more rigorously whether the periodically pitched stator can improve stage performance, an example with compressible flow is studied in this section. Based on the immersed-boundary method, the compressible conversation equations of mass, momentum, and energy are solved. The governing equations are written as

$$\frac{\partial \rho}{\partial t} + \frac{\partial}{\partial x_j}(\rho u_j) = 0 \tag{7}$$

$$\frac{\partial \rho u_i}{\partial t} + \frac{\partial}{\partial x_j}(\rho u_j u_i) = -\frac{\partial p}{\partial x_i} + \frac{\partial \tau_{ij}}{\partial x_j} + \sum_{l=1}^{M} \boldsymbol{F}_l \tag{8}$$

$$\frac{\partial}{\partial t}\left[\rho\left(e + \frac{u_i u_i}{2}\right)\right] + \frac{\partial}{\partial x_j}\left[\rho u_j\left(h + \frac{u_i u_i}{2}\right)\right] = \frac{\partial}{\partial x_j}(u_i \hat{\tau}_{ij}) \tag{9}$$

where e is the internal energy, h is the enthalpy, $\hat{\tau}_{ij}$ is the viscous stress tensor, $\boldsymbol{F}_l$ denotes the boundary forces, and the k-ε model is used to consider Reynolds stress tensors. The same numerical scheme is used in the study of Du et al. [23]. A stage consisting of 2:3 rotor–stator blades is investigated, as depicted in Fig. 29. The blade is NACA 2606, and the chord is 0.1. The parameters are given in Table 5, where $Ma_r = |V|/c_0$ is the Mach number, and c_0 is speed of sound. At the inlet, the total pressure, total temperature, and velocity angle are specified for the boundary conditions. At the exit, the static pressure is specified.

Table 3 Blade, flow, and geometric parameters of pitching IGV

α_1	α_2	α_3	Re	l	U	d_1	d_2	δ_1
−15 deg	45 deg	−45 deg	500	0.3c	0.20–0.45	0.95	0.85	0.05c

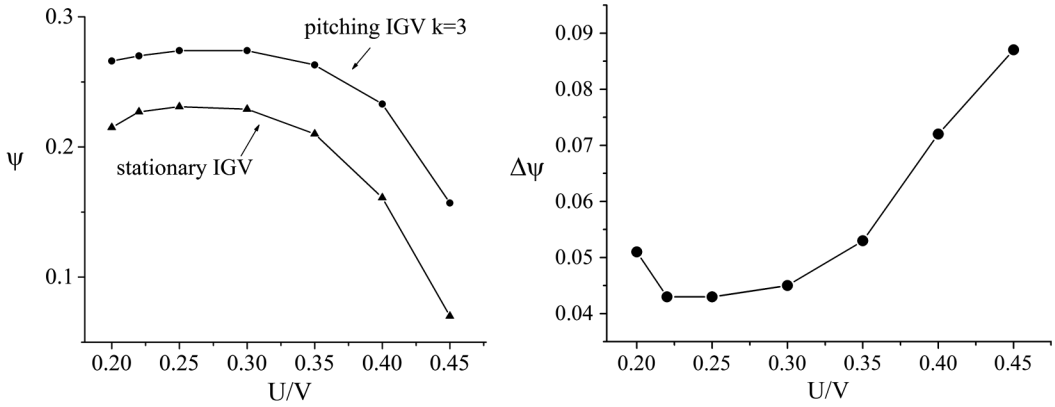

Fig. 26 Comparison of ψ and $\Delta\psi$ vs flow coefficient: stationary and pitching IGV.

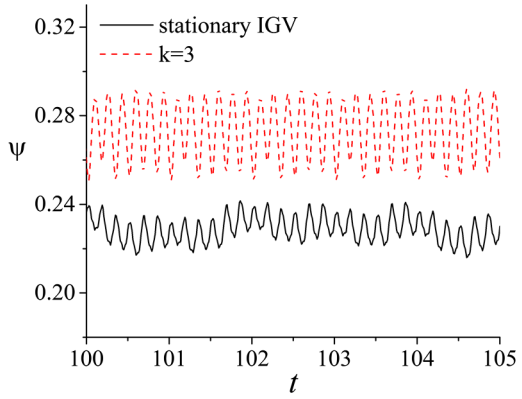

Fig. 27 Comparison of unsteady stage total pressure rise: pitching and stationary IGV.

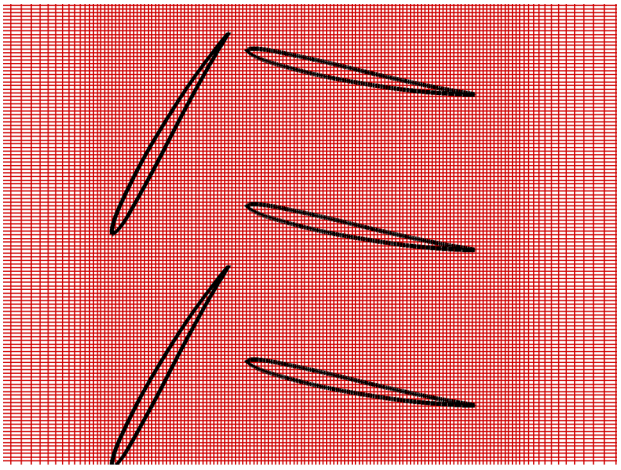

Fig. 29 Configuration of 2:3 rotor/stator. NACA 2606 blade. $\alpha_1 = 58$ deg, $\alpha_2 = -20$ deg, $l = 0.5c, \delta = 0.07c$.

Figure 30 shows a comparison of static pressure rise for the stationary and pitching stators with an optimized pitching phase, as obtained by specifying the outlet static pressure. The stagger angle of the stator blades is pitched between −17 and −20 deg. The stage performance is improved by the interaction between the rotor and pitched stator blades with optimal pitching phase. For $U/V = 0.29$, the average lift coefficient is enhanced from 0.286 to 0.314, which represents a significant enhancement of stage loading. The stage static pressure rise at one chord after the trailing edge of the stator is enhanced from 0.415 to 0.455, and the amplitude of fluctuation increases from 0.022 to 0.041.

As compared to results with the stationary stator, very high unsteady lift peaks are generated by the rotor/pitching-stator interaction for $U/V = 0.29$, as depicted in Fig. 31. Figure 32 shows a comparison of the vorticity field for three different instants around the rotor lift peak. The vortex around the trailing edge of the rotor blade is enhanced at these instants, as observed in the laminar and incompressible flow example. As described with respect to Fig. 2, on the basis of Kelvin's theorem, when a vortex sheds from the blade, a circulation is generated around the blade. For the same inflow and rotational velocity, Fig. 31 shows that higher lift can be obtained, due to the increase in circulation. At this instant, the lift coefficient peak is increased from 0.43 to 0.61, and the maximum

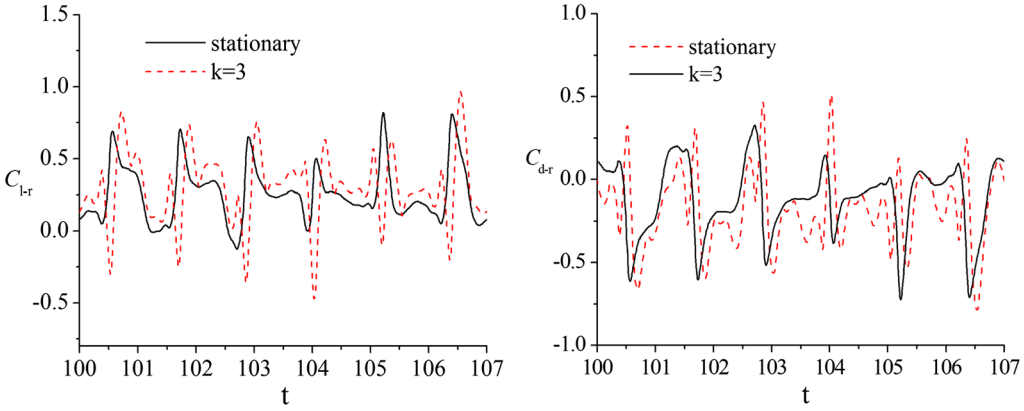

Fig. 28 Comparison of lift and drag coefficients on rotor blades in given period ($T = 7$).

Table 4 Stage total pressure rise for different stagger angles of stator blades (IGV)

Parameter	Values			
α_1, deg	-8	−12	−15	−8 to −15 ($k = 3$)
ψ	0.228	0.227	0.227	0.274
Amplitude of ψ_t	0.011	0.011	0.017	0.020

Table 5 Blade, flow, and geometric parameters of compressible flow configuration (Fig. 29)

α_1	α_2	Re	Ma_r	l	δ
58 deg	−20 deg	2×10^5	0.27	$0.5c$	$0.07c$

vorticity near the trailing edge is increased from 2.62×10^3 to 3.47×10^3. Like the high unsteady vortex lift generated in the motion of an insect, the unsteady vortex here plays a very important role in increasing stage loading. If the rotor/pitching-stator stage is designed with proper pitching phase and amplitude, performance can be improved through the application of the unsteady vortex lift mechanism.

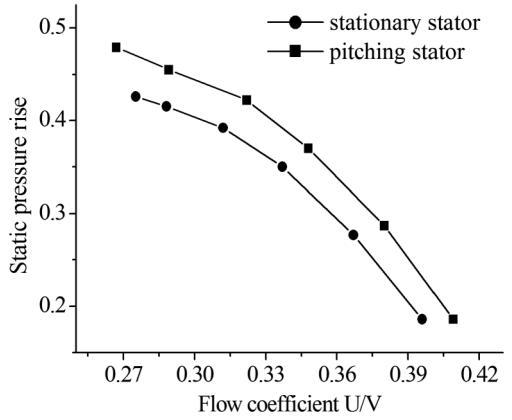

Fig. 30 Comparison of static pressure rise for stationary vs pitching stator.

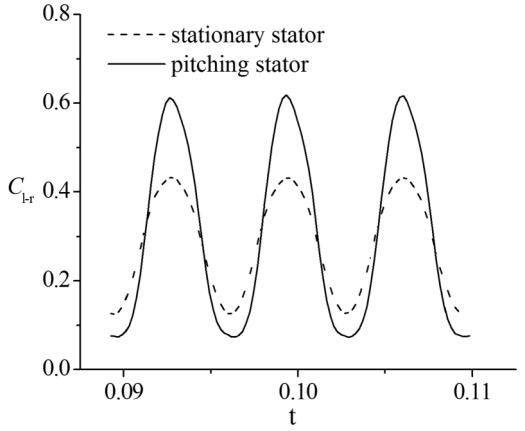

Fig. 31 Comparison of rotor lift coefficient for stationary vs pitching stators with $U/V = 0.29$.

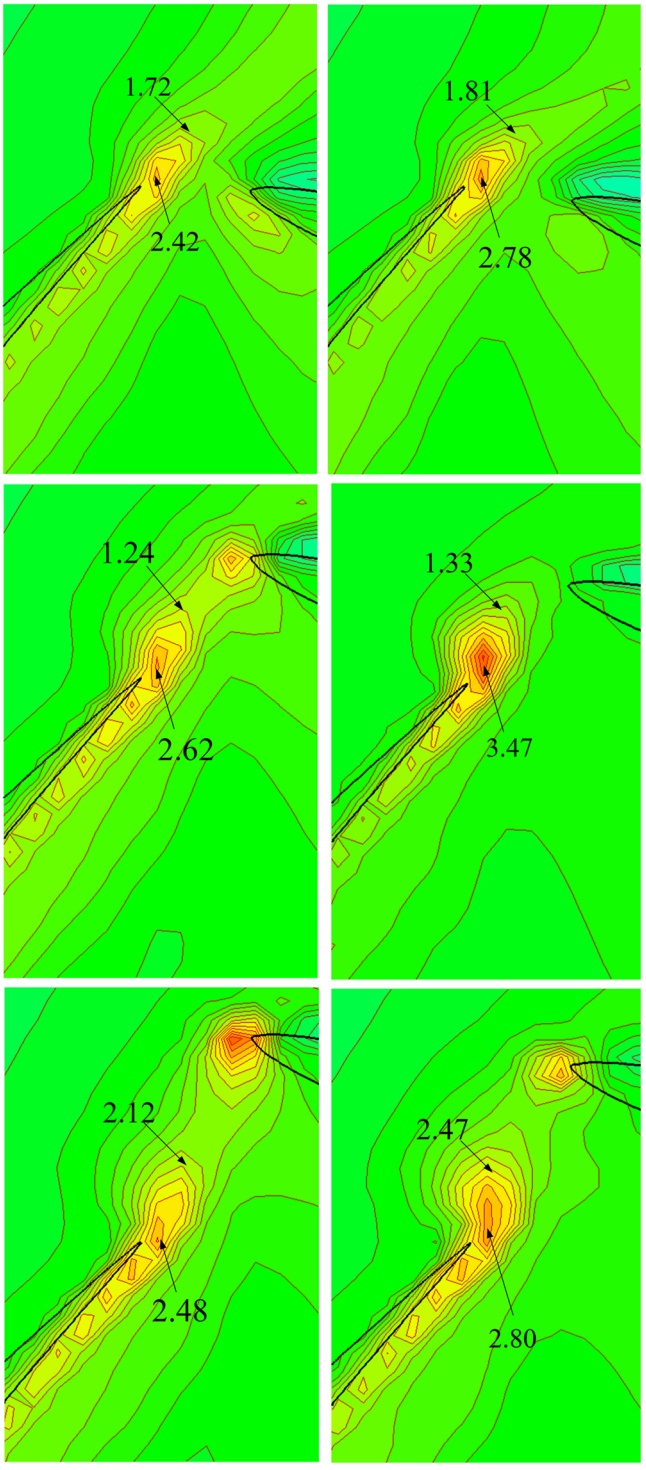

Fig. 32 Comparison of vorticity field ($\omega \cdot 10^{-3}$) between stationary stator and pitching stator at instants of lift peak with $U/V = 0.29$.

V. Conclusions

It has become increasingly difficult to enhance the loading of a turbomachine based on conventional aerodynamic theories. Research on insect flight shows, however, that high unsteady lift can be generated by imitating the hovering motion of insects. Inspired by previous studies on the fore- and hindwing interaction in dragonfly flight, the present work proposes a novel stage consisting of a rotor and a pitching stator that will take advantage of unsteady lift. Flow associated with the rotor/pitching stator is very complex and difficult to calculate, however, because of the relative motion between rotor and pitching stator. Based on the immersed-boundary

method, a new numerical scheme is developed to avoid the grid regeneration for this type of moving boundary problem and reduce the errors arising from the interface between blade rows. The scheme is used to simulate the evolution of unsteady vortices between rotor/pitching-stator rows.

In the present work, the relation between unsteady vortices, rotor lift coefficient, and stage pressure rise is simulated. The numerical results indicate that the stage loading can be enhanced by the interaction between the rotor and pitched stator, which influences the distribution of unsteady vortices around the rotor blades. The effects of pitching stator blades are not limited to the local area but are seen throughout the rotor–stator system. The most crucial parameter in the present system is the relative phase between the rotor and the periodically pitched stator blade, similar to the phase between the fore- and the hindwing in dragonfly flight. The relative phase determines whether the effect of the rotor/pitching stator is positive or negative. The average lift coefficient of the rotor blade is increased by the pitching stator if the relative phase between rotor and pitching stator is optimized. Lift peaks are generated for each rotor blade in turn as it interacts with the pitching stators, which leads to an increase in average loading. The analysis of the unsteady flowfield shows us that the high unsteady lift is related to the unsteady vortices shedding from the blades. The stage performance is also influenced by the pitching amplitude coefficient A, axial gap, and flow coefficient. A thorough parametric investigation is performed in this study.

The rotor/pitching-stator system for implementation of unsteady lift is a novel design for turbomachinery, and the present work shows its promise. Future work should consider a number of aspects of this configuration, and comparative experiments should be performed.

Acknowledgments

The financial support of the National Natural Science Foundation of China (grants 51236001 and 51076006) and the 973 Program (grant 2012CB720200) are gratefully acknowledged.

References

[1] Weis-Fogh, T., "Quick Estimates of Flight Fitness in Hovering Animals Including Novel Mechanism for Lift Production," *Journal of Experiment Biology*, Vol. 31, 1973, pp. 169–230.

[2] Lighthill, M. J., "On the Weis-Fogh Mechanism of Lift Generation," *Journal of Fluid Mechanics*, Vol. 60, No. 6, 1973, pp. 1–17. doi:10.1017/S0022112073000017

[3] Maxworthy, T., "Experiments on the Weis-Fogh Mechanism of Lift Generation by Insects in Hovering Flight. Part 1. Dynamics of the Fling," *Journal of Fluid Mechanics*, Vol. 93, 1979, pp. 47–63. doi:10.1017/S0022112079001774

[4] Spedding, G. R., and Maxworthy, T., "The Generation of Circulation and Lift in a Rigid Two-Dimensional Fling," *Journal of Fluid Mechanics*, Vol. 165, No. 6, 1986, 247–272. doi:10.1017/S0022112086003087

[5] Edwards, R. H., and Cheng, H. K., "The Separation Vortex in the Weis-Fogh Circulation-Generation Mechanism," *Journal of Fluid Mechanics*, Vol. 120, No. 6, 1982, pp. 463–473. doi:10.1017/S0022112082002857

[6] Dickinson, M. H., and Götz, K. G., "Unsteady Aerodynamic Performance of Model Wings at Low Reynolds Numbers," *Journal of Experiment Biology*, Vol. 174, 1993, pp. 45–64.

[7] Dickinson, M. H., Lehmann, F. O., and Sane, S. P., "Wing Rotation and the Aerodynamic Basis of Insect Flight," *Science*, Vol. 284, No. 5422, 1999, pp. 1954–1960. doi:10.1126/science.284.5422.1954

[8] Wang, Z. J., Birch, J. M., and Dickinson, M. H., "Unsteady Forces and Flows in Low Reynolds Number Hovering Flight: Two-Dimensional Computations vs Robotic Wing Experiments," *Journal of Experimental Biology*, Vol. 207, No. 3, 2004, pp. 449–460. doi:10.1242/jeb.00739

[9] Miller, L. A., and Peskin, C. S., "When Vortices Stick: An Aerodynamic Transition in Tiny Insect Flight," *Journal of Experiment Biology*, Vol. 207, No. 17, 2004, pp. 3073–3088. doi:10.1242/jeb.01138

[10] Li, G.-J., and Lu, X.-Y., "Force and Power of Flapping Plates in a Fluid," *Journal of fluid Mechanics*, Vol. 712, Dec. 2012, pp. 598–613. doi:10.1017/jfm.2012.443

[11] Sun, M., and Lan, S. L., "A Computational Study of the Aerodynamic Forces and Power Requirements of Dragonfly Hovering," *Journal of Experimental Biology*, Vol. 207, 2004, pp. 1887–1901.

[12] Wang, J. K., and Sun, M., "A Computational Study of the Aerodynamic and Forewing–Hindwing Interaction of a Model Dragonfly in Forward Flight," *Journal of Experimental Biology*, Vol. 208, Pt. 19, 2005, pp. 3785–3804.

[13] Alexander, D. E., "Unusual Phase Relationships Between the Forewings and Hind Wings in Flying Dragonflies," *Journal of Experimental Biology*, Vol. 109, 1984, pp. 379–383.

[14] Ellington, C. P., "The Aerodynamics of Hovering Insect Flight. 1–5," *Philosophical Transactions of the Royal Society of London, Series B*, Vol. 305, 1984, pp. 1–181.

[15] Norberg, R.A., "Hovering Flight of the Dragonfly Aeschna Juncea L., Kinematics and Aerodynamics," *Swimming and Flying in Nature*, edited by Wu, T.Y., Brokaw, C. J., and Brennen, C., Vol. 2, Plenum Press, New York, 1975, pp. 763–781.

[16] Wang, Z. J., "Dissecting Insect Flight," *Annual Review of Fluid Mechanics*, Vol. 37, 2005, pp. 183–210. doi:10.1146/annurev.fluid.36.050802.121940

[17] Wang, Z. J., and Russell, D., "Effect of Forewing and Hindwing Interactions on Aerodynamic Forces and Power in Hovering Dragonfly Flight," *Physical Review Letters*, Vol. 99, No. 14, 2007, p. 148101.

[18] Zhang, J., and Lu, X.-Y., "Aerodynamic Performance Due to Forewing and Hindwing Interaction in Gliding Dragonfly Hovering," *Physical Review E*, Vol. 80, No. 6, 2009, Paper 017302.

[19] Shyy, W., Aono, H., Chimakurthi, S. K., Trizila, P., Kang, C.-K., Cesnik, C. E. S., and Liu, H., "Recent Progress in Flapping Wing Aerodynamics and Aeroelasticity," *Progress in Aerospace Sciences*, Vol. 46, No. 7, 2010, pp. 284–327. doi:10.1016/j.paerosci.2010.01.001

[20] Tsutahara, M., and Kimura, T., "An Application of the Weis-Fogh Mechanism to Ship Propulsion," *ASME Journal of Fluids Engineering*, Vol. 109, No. 2, 1987, pp. 107–113. doi:10.1115/1.3242629

[21] Tsutahara, M., Kimura, T., and Ro, K., "Ship's Propulsion Mechanism of Two-Stage 'Weis-Fogh' Type," *ASME Journal of Fluids Engineering*, Vol. 116, No. 2, 1994, pp. 278–286. doi:10.1115/1.2910267

[22] Furber, S. B., and Ffowcs Williams, J. E., "Is the Weis-Fogh Principle Exploitable in Turbomachinery" *Journal of Fluid Mechanics*, Vol. 94, No. 3, 1979, pp. 519–540. doi:10.1017/S0022112079001166

[23] Du, L., Sun, X., and Yang, V., "Generation of Vortex Lift by Reducing Rotor–Stator Axial Gap in Turbomachinery," *Journal of Propulsion and Power* (submitted for publication).

[24] Yamada, K., Funazaki, K., Kikuchi, M. , and Sato, H., "Influences of Axial Gap Between Blade Rows on Secondary Flows and Aerodynamic Performance in a Turbine Stage," *Proceedings of ASME Turbo Expo 2009: Power for Land, Sea and Air*, American Soc. of Mechanical Engineers Paper GT2009-59855, New York, 2009.

[25] Funazaki, K., Yamada, K., Kikuchi, M., and Sato, H., "Experimental Studies on Aerodynamic Performance and Unsteady Flow Behaviors of a Single Turbine Stage with Variable Rotor–Stator Axial Gap: Comparisons with Time-Accurate Numerical Simulation," *ASME Turbo Expo 2007: Power for Land, Sea and Air*, American Soc. of Mechanical Engineers Paper GT2007-27670, New York, 2007.

[26] Gaetani, P., Persico, G., Dossena, V., and Osnaghi, C., "Investigation of the Flow Field in a High-Pressure Turbine Stage for Two Stator-Rotor Axial Gaps – Part 1: Three Dimensional Time-Averaged Flow Field," *Transaction of ASME, Journal of Turbomachinery*, Vol. 129, No. 3, 2007, pp. 572–579. doi:10.1115/1.2472383

[27] Smith, L., "Wake Dispersion in Turbomachines," *Journal of Basic Engineering*, Vol. 88, No. 3, 1966, pp. 688–690. doi:10.1115/1.3645942

[28] Zheng, X.-Q., Zhou, S., Hou, A.-P. , and Xiong, J.-S., "Compressibility Effects on the Two Generations of Unsteady Flow Types in Axial Flow Compressors," *ASME Turbo Expo 2005: Power for Land, Sea and Air*, American Soc. of Mechanical Engineers Paper GT2005-68928, New York, 2005.

[29] Rai, M. M., "Unsteady Three-Dimensional Navier–Stokes Simulations of Turbine Rotor–Stator Interaction," *23rd Joint Propulsion Conference*, AIAA Paper 1987-2058, 1987.

[30] Rai, M. M., "A Conservative Treatment of Zonal Boundaries for Euler Equation Calculations," *Journal of Computational Physics*, Vol. 62, No. 2, 1986, pp. 472–503. doi:10.1016/0021-9991(86)90141-5

[31] Jorgenson, P., C. E., and Chima, R.V., "An Explicit Runge–Kutta Method for Unsteady Rotor/Stator Interaction," *26th Aerospace Sciences Meeting*, AIAA Paper 1988-0049, 1988.
[32] Chima, R. V., "Explicit Multigrid Algorithm for Quasi-Three-Dimensional Viscous Flows in Turbomachinery," *Journal of Propulsion and Power*, Vol. 3, No. 5, 1987, pp. 397–405. doi:10.2514/3.23004
[33] Giles, M. B., "Calculation of Unsteady Wake/Rotor Interaction," *Journal of Propulsion and Power*, Vol. 4, No. 4, 1988, pp. 356–362. doi:10.2514/3.23074
[34] Hirt, C. W., and Nichols, B. D., "Volume of Fluid (VOF) Method for the Dynamics of Free Boundaries," *Journal of Computational Physics*, Vol. 39, No. 6, 1981, pp. 201–225. doi:10.1016/0021-9991(81)90145-5
[35] Osher, S., and Sethian, J. A., "Fronts Propagating with Curvature-Dependent Speed: Algorithms Based on Hamilton–Jacobi Formulations," *Journal of Computational Physics*, Vol. 79, No. 6, 1988, pp. 12–49. doi:10.1016/0021-9991(88)90002-2
[36] Eldredge, J. D., Leonard, A., and Colonius, T., "A General Deterministic Treatment of Derivatives in Particle Methods," *Journal of Computational Physics*, Vol. 180, No. 2, 2002, pp. 686–709. doi:10.1006/jcph.2002.7112
[37] Eldredge, J. D., "Numerical Simulation of the Fluid Dynamics of 2D of Rigid Body Motion with the Vortex Particle Method," *Journal of Computational Physics*, Vol. 221, No. 2, 2006, pp. 626–648. doi:10.1016/j.jcp.2006.06.038
[38] Cottet, G.-H., and Koumoutsakos, P., *Vortex Methods: Theory and Practice*, Cambridge Univ. Press, Cambridge, England, U.K., 2000, pp. 10–205.
[39] Peskin, C. S., "Numerical Analysis of Blood Flow in the Heart," *Journal of Computational Physics*, Vol. 25, No. 3, 1977, pp. 220–252. doi:10.1016/0021-9991(77)90100-0
[40] Goldstein, D., Handler, R., and Sirovich, L., "Modeling a No-Slip Flow Boundary with an External Force Field," *Journal of Computational Physics*, Vol. 105, No. 2, 1993, pp. 354–366. doi:10.1006/jcph.1993.1081
[41] Ming-Chih, L., and Peskin, C. S., "An Immersed Boundary Method with Formal Second-Order Accuracy and Reduced Numerical Viscosity," *Journal of Computational Physics*, Vol. 160, No. 2, 2000, pp. 705–719. doi:10.1006/jcph.2000.6483
[42] Zhong, G, and Sun, X., "New Simulation Strategy for an Oscillating Cascade in Turbomachinery Using Immersed-Boundary Method," *Journal of Propulsion and Power*, Vol. 25, No. 2, 2009, pp. 312–321. doi:10.2514/1.35347
[43] Du, L., Jing, X., and Sun, X., "Modes of Vortex Formation and Transition to Three-Dimensionality in the Wake of a Freely Vibrating Cylinder," *Journal of Fluids and Structure*, Vol. 49, Aug. 2014, 554–573. doi:10.1016/j.jfluidstructs.2014.05.012
[44] Du, L., and Sun, X., "Suppression of Vortex-Induced Vibration Using the Rotary Oscillation of a Cylinder," *Physics of Fluids*, Vol. 27, No. 2, 2015, Paper 023603. doi:10.1063/1.4913353
[45] Du, L., Jing, X., Sun, X., and Song, W., "Aeroacoustic Model of a Modulation Fan with Pitching Blades as a Sound Generator," *Journal of the Acoustical Society of America*, Vol. 136, No. 4, 2014, pp. 1542–1551. doi:10.1121/1.4893904
[46] Park, J., and Garcés, M., "The Rotary Subwoofer: A Controllable Infrasound Source," *Journal of the Acoustical Society of America*, Vol. 125, No. 4, 2009, pp. 2006–2012. doi:10.1121/1.3082115

F. Liu
Associate Editor